PCCP

Accepted Manuscript




ROYAL SOCIETY OF CHEMISTRY

www.rsc.org/pccp

# MOLECULAR DYNAMICS SIMULATION OF PLANAR ELONGATIONAL FLOW IN A NEMATIC LIQUID CRYSTAL BASED ON THE GAY-BERNE POTENTIAL

Sten Sarman and Aatto Laaksonen
Department of Materials and Environmental Chemistry
Arrhenius Laboratory
Stockholm University
106 91 Stockholm
SWEDEN

**ABSTRACT**

Molecular dynamics simulations of planar elongational flow in a nematic liquid crystal model system based on the Gay-Berne fluid were undertaken by applying the SLLOD equations of motion with an elongational velocity field or strain rate. In order to facilitate the simulation, Kraynik-Reinelt periodic boundary conditions allowing indefinite simulations were used. A Lagrangian constraint algorithm was utilized to fix the director at different angles relative to the elongation direction, so that the various pressure tensor elements could be calculated as a function of this angle. This made it possible to obtain accurate values of the shear viscosities which were found to agree with results previously obtained by shear flow simulations. The torque needed to fix the director at various angles relative to the elongation direction was evaluated in order to determine the stable orientation of the director, where this torque is equal to zero. This orientation was found to be parallel to the elongation direction. It was also noted that the irreversible entropy production was minimal when the director attained this orientation. Since the simulated system was rather large and fairly long simulation runs were undertaken it was also possible to study the cross coupling between the strain rate and the order tensor. It turned out to be very weak at low strain rates but at higher strain rates it could lead to break down of the liquid crystalline order.

## 1. INTRODUCTION

Viscosities and shear flow of liquids have been studied by molecular dynamics simulation since the 1970's, when the Lees Edwards sliding brick boundary conditions were introduced to induce a shear stress and a velocity gradient [1]. Then the viscosity can be obtained as the ratio of these two quantities. At first simple liquids such as Lennard-Jones liquids were examined but then the simulations have been extended to more complex systems such as, for example, alkanes [2-4] that are of more practical interest since they, among other things, are constituents of lubricants. Also the flow properties of liquid crystals [5-8] have been studied. The simulation methodology was improved by the introduction of the SLLOD equations of motion [9] where the molecular velocity is divided into the streaming velocity and the molecular thermal velocities, where the average of the sum of the squares of the latter velocities is proportional to the temperature. The SLLOD equations are an exact description of adiabatic shear flow and in the limit of zero shear rate the viscosity is equal to the viscosity in the linear or Newtonians regime also given by the Green-Kubo relation. When these equations are augmented with a thermostat they can also be used to study non-Newtonian flow. Apart from obtaining numerical values of the viscosity it is also possible study various flow alignment phenomena. For example, the director of nematic liquid crystals orient at a constant angle relative to the stream lines [7, 8] and linear molecules such as alkanes are stretched out and aligned by the shear field thus becoming a kind of a nonequilibrium liquid crystal [2-4].

One flow pattern that has been considerably less studied is elongational flow. It arises when a system is elongated in one direction and contracts in a perpendicular direction while the volume of the system remains constant. It is divergence free and irrotational. It is of technological interest in, for example, polymer processing operations such as spinning, extrusion, vacuum forming and flow close to a tank inlet or outlet. Elongational flow can also be studied by applying the SLLOD equations of motion with an elongational velocity field replacing the shear field. However, special care has to be taken when the periodic boundary conditions are selected and this could be one of the reasons why this flow has attracted less attention. The simplest applicable periodic boundary conditions consist of a lattice of unit cells contracting in one direction and expanding in the perpendicular direction but then the simulation can only continue as long as the width of the simulation cell exceeds twice the range of the intermolecular interaction potential and thus there is definite length of the simulation. This could be enough if only short simulations are needed but it will be difficult to study transport phenomena, where longer simulations are necessary. This obstacle was overcome by Daivis and Todd [10, 11] and by Baranyai and Cummings [12] utilizing two facts: Firstly, it is possible to ap-

ply a theorem of Kraynik and Reinelt [13], according to which there is more than one equivalent representation of a two-dimensional periodic lattice. In particular a lattice of quadratic unit cells can be represented by a lattice of unit cells shaped like parallelograms where the latter lattice can be exactly mapped onto the former lattice. Secondly, if the expansion and contraction directions of the elongational flow are oblique relative to the sides of the initial quadratic unit cells, they are transformed to parallelograms. Then it is possible to choose the elongation and contraction direction in such a way, that a lattice of parallelograms that can be remapped to the original lattice of quadratic unit cells forms after a certain simulation time and thus the simulation can continue indefinitely. These boundary conditions are easy to implement in an existing molecular dynamics simulation program, so that elongational flow can be simulated just as readily as shear flow.

So far elongational flow of simple liquids such as Lennard-Jones liquids [14], low molecular liquids [15] and of polymer melts have been investigated [16, 17], and the purpose of this work is to extend these studies to a liquid crystal model system based on the Gay-Berne potential [18-20] in order to evaluate the shear viscosities and to study alignment phenomena. The article is organized in the following way: In section 2 the necessary theory is reviewed, in sections 3 the model system is described, in section 4 the results are presented and discussed and finally in section 5 there is a conclusion.

## 2. THEORY

### 2a. Order Parameter

The degree of ordering in a liquid crystal can be characterised by the scalar order parameter and a measure of the average orientation is given by the director. Many properties of an axially symmetric system such as a nematic liquid crystal become simpler when they are expressed relative to a director based coordinate system. These quantities can be defined by introducing the order tensor,

$$\mathbf{Q} = \frac{3}{2}\left( \frac{1}{N}\sum_{i=1}^{N} \hat{\mathbf{u}}_i \hat{\mathbf{u}}_i - \frac{1}{3}\mathbf{1} \right) \tag{2.1}$$

where $N$ is the number of molecules in the system, $\{\hat{\mathbf{u}}_i; 1 \le i \le N\}$ is the unit vector in the direction of the axis of revolution of the molecule and $\mathbf{1}$ is the unit second rank tensor. Then the largest eigenvalue of this tensor is defined as the order parameter $S$. When the molecules are perfectly aligned in the same direction the order parameter is equal to unity and when the orientation is completely random it is equal to zero. The director $\mathbf{n}$ is the eigenvector corre-

sponding to the order parameter. In terms of the director and the order parameter the order tensor may also be expressed as

$$\mathbf{Q} = \frac{3}{2} S\left( \mathbf{nn} - \frac{1}{3}\mathbf{1} \right). \tag{2.2}$$

The order parameter and the director are functions of the position in space in a macroscopic system, but in this work we will only be interested in small systems where these quantities are the same over the whole system. The director angular velocity is given by

$$\boldsymbol{\Omega} = \mathbf{n} \times \dot{\mathbf{n}} . \tag{2.3}$$

**2b. Linear phenomenological relations**

In order to obtain the linear relation between the various thermodynamic forces and fluxes in a flowing liquid crystal, we start with the expression for the irreversible entropy production of a liquid crystal undergoing a flow in general [21, 22],

$$\sigma = -\frac{1}{T}\left\{ \left\langle \overset{\circ}{\mathbf{P}}{}^{s} \right\rangle : (\overset{\circ}{\nabla}\mathbf{u})^{s} \; + 2\left\langle \mathbf{P}^{a} \right\rangle \cdot (½\nabla \times \mathbf{u} - \boldsymbol{\Omega}) + \left\langle (1/3)\mathrm{Tr}(\mathbf{P}) - p_{eq} \right\rangle \nabla \cdot \mathbf{u} \right\}, \tag{2.4}$$

where $T$ is the absolute temperature, $\mathbf{u}$ is the streaming velocity, $\mathbf{P}$ is the pressure tensor, $\boldsymbol{\Omega}$ is the director angular velocity and $p_{eq}$ is the equilibrium pressure. The three pairs of thermodynamic forces and fluxes are (*i*) the symmetric traceless pressure tensor and the strain rate, $\left\langle \overset{\circ}{\mathbf{P}}{}^{s} \right\rangle$ and $(\overset{\circ}{\nabla}\mathbf{u})^{s}$, where a symmetric traceless part of a general tensor $\mathbf{A}$ is defined as $\mathring{\mathbf{A}}^{s} = (1/2)(\mathbf{A} + \mathbf{A}^{T}) - (1/3)\mathrm{Tr}(\mathbf{A})\mathbf{1}$ and $\mathbf{1}$ is the unit tensor, (note that the strain rate is the same as the symmetric traceless part of the velocity gradient), (*ii*) the pseudo vector dual of the antisymmetric pressure tensor and the difference between the director angular velocity and the rotational part of the streaming velocity, $\left\langle \mathbf{P}^{a} \right\rangle$ and $(½\nabla \times \mathbf{u} - \boldsymbol{\Omega})$, where the pseudovector dual of the antisymmetric part of a general tensor $\mathbf{A}$ is given by $\mathbf{A}^{a} = (1/2)\boldsymbol{\varepsilon} : \mathbf{A}$, where $\boldsymbol{\varepsilon}$ is the isotropic third rank tensor or the Levi-Civita tensor, and finally (*iii*) the difference between the trace of the pressure tensor and the equilibrium pressure and the divergence of the streaming velocity $\left\langle (1/3)\mathrm{Tr}(\mathbf{P}) - p_{eq} \right\rangle$ and $\nabla \cdot \mathbf{u}$. The forces are externally given parameters whereas the fluxes are ensemble averages of phase functions, hence the angular brackets.

In an axially symmetric system such as a nematic liquid crystal the most general expression for the linear relation between the pressure tensor and the velocity gradient can be expressed in the following way [21-23],

$$\left\langle \overset{\circ}{\mathbf{P}}{}^{s} \right\rangle = -2\eta(\overset{\circ}{\nabla}\mathbf{u})^{s} - 2\tilde{\eta}_{1}[(\overset{\circ}{\mathbf{nn}})^{s} \cdot (\overset{\circ}{\nabla}\mathbf{u})^{s}]^{s} - 2\tilde{\eta}_{3}(\overset{\circ}{\mathbf{nn}})^{s}[(\overset{\circ}{\mathbf{nn}})^{s} : (\overset{\circ}{\nabla}\mathbf{u})^{s}]$$

$$+\ \ 2\tilde{\eta}_2[(\overset{\circ}{\mathbf{nn}})^s\cdot\boldsymbol{\varepsilon}\cdot(\tfrac{1}{2}\boldsymbol{\nabla}\times\mathbf{u}-\boldsymbol{\Omega})]^s-\ \zeta(\overset{\circ}{\mathbf{nn}})^s\boldsymbol{\nabla}\cdot\mathbf{u}\,, \tag{2.5a}$$

$$\left\langle\mathbf{P}^a\right\rangle\ =\ -\frac{\tilde{\gamma}_1}{2}(\mathbf{1}-\mathbf{nn})\cdot(\tfrac{1}{2}\boldsymbol{\nabla}\times\mathbf{u}-\boldsymbol{\Omega})-\frac{\tilde{\gamma}_2}{2}[(\overset{\circ}{\mathbf{nn}})^s\ \cdot(\overset{\circ}{\boldsymbol{\nabla}}\mathbf{u})^s\ ] \tag{2.5b}$$

and

$$(1/3)\left\langle\mathrm{Tr}(\mathbf{P})\right\rangle-p_{eq}=-\eta_V\boldsymbol{\nabla}\cdot\mathbf{u}\ \ -\ \ \kappa(\overset{\circ}{\mathbf{nn}})^s:(\overset{\circ}{\boldsymbol{\nabla}}\mathbf{u})^s\,, \tag{2.5c}$$

where the quantities $\eta$, $\tilde{\eta}_1$ and $\tilde{\eta}_3$ are shear viscosities, $\tilde{\gamma}_1$ is the twist viscosity, $\eta_V$ is the volume viscosity, $\tilde{\eta}_2$ is the cross coupling coefficient between the difference between the rotation of the streaming velocity and the director angular velocity and the symmetric traceless pressure. According to the Onsager reciprocity relations (ORR) [24] this coefficient is equal to $\tilde{\gamma}_2/2$, the cross coupling coefficient between the strain rate and the antisymmetric pressure. The trace of the velocity gradient and the symmetric traceless pressure are related by the cross-coupling coefficient $\zeta$, which, according to the ORR, is equal to the cross-coupling coefficient $\kappa$ between the strain rate and the difference between the trace of the pressure tensor and the equilibrium pressure. In the case of planar elongational flow the above equations can be shortened since the only thermodynamic force is the strain rate $(\overset{\circ}{\boldsymbol{\nabla}}\mathbf{u})^s$, so that only those terms that involve this quantity remain in equation (2.5).

In order to further simplify the relation (2.5) in the case of planar elongational flow it is useful to define three different coordinate systems: Firstly, we start with one original coordinate system with the basis vectors $(\mathbf{e}_x,\mathbf{e}_y,\mathbf{e}_z)$ used in the actual calculations. Secondly, we define a coordinate system with the basis vectors $(\mathbf{e}'_x,\mathbf{e}'_y\,\mathbf{e}'_z)$ by rotation around the *y*-axis, so that *x*-axis becomes parallel to the elongation direction $\mathbf{e}'_x$, $\mathbf{e}'_y=\mathbf{e}_y$ and the contraction direction becomes parallel to $\mathbf{e}'_z$. The angle between $\mathbf{e}'_x$ and $\mathbf{e}_x$ is denoted by $\varphi$ and it is positive for a rotation clockwise around the *y*-axis from $\mathbf{e}_x$ to $\mathbf{e}'_x$. In this coordinate system the angle between the director $\mathbf{n}$ and $\mathbf{e}'_x$ is $\theta'$ and it is positive when the director is rotated clockwise from $\mathbf{e}'_x$. Thirdly, we introduce a director based coordinate system with the basis vectors $(\mathbf{e}_1,\mathbf{e}_2\,\mathbf{e}_3)$ obtained by rotation around the *y*-axis, where $\mathbf{e}_1$ is parallel to the director $\mathbf{n}$, $\mathbf{e}_2=\mathbf{e}'_y=\mathbf{e}_y$ is parallel to the *y*-axis, and $\mathbf{e}_3=\mathbf{n}\times\mathbf{e}_2$. The angle between $\mathbf{e}_1$ and $\mathbf{e}'_x$ is denoted by $\theta$ and it is positive for a rotation clockwise around the *y*-axis from $\mathbf{e}_1$ to $\mathbf{e}'_x$ so we have $\theta=-\theta'$, see fig. 1.

The relation between the various pressure tensor element and the strain rate become simpler in the director based coordinate system where $\mathbf{e}'_x = \mathbf{e}_1 \cos\theta - \mathbf{e}_3 \sin\theta$, $\mathbf{e}'_z = \mathbf{e}_1 \sin\theta + \mathbf{e}_3 \cos\theta$ and $\mathbf{e}'_y = \mathbf{e}_2 = \mathbf{e}_y$. Then the strain rate becomes:

$$(\overset{\circ}{\boldsymbol{\nabla}}\mathbf{u})^s = \gamma(\mathbf{e}'_x\mathbf{e}'_x - \mathbf{e}'_z\mathbf{e}'_z) = \gamma \begin{pmatrix} \cos 2\theta & 0 & -\sin 2\theta \\ 0 & 0 & 0 \\ -\sin 2\theta & 0 & -\cos 2\theta \end{pmatrix}, \tag{2.6}$$

and only the following components of the pressure tensor are left:

$$\left\langle \overset{\circ}{p}{}^s_{11} \right\rangle = -\left( 2\eta + \frac{2\tilde{\eta}_3}{3} \right) \gamma \cos 2\theta, \tag{2.7a}$$

$$\left\langle \overset{\circ}{p}{}^s_{22} \right\rangle = -\frac{2}{3}(\tilde{\eta}_1 + \tilde{\eta}_3)\gamma \cos 2\theta, \tag{2.7b}$$

$$\left\langle \overset{\circ}{p}{}^s_{33} \right\rangle = \left( 2\eta + \frac{2\tilde{\eta}_1}{3} + \frac{4\tilde{\eta}_3}{3} \right) \gamma \cos 2\theta, \tag{2.7c}$$

$$\left\langle \overset{\circ}{p}{}^s_{31} \right\rangle = \left( 2\eta + \frac{\tilde{\eta}_1}{3} \right) \gamma \sin 2\theta \tag{2.7d}$$

and

$$2\left\langle p^a_2 \right\rangle = \left\langle \hat{\lambda}_2 \right\rangle = -\tilde{\gamma}_2 \gamma \sin 2\theta. \tag{2.7e}$$

This means that all the shear viscosities and the cross coupling coefficient between the strain rate and the antisymmetric pressure can be obtained by simulating an elongational flow.

Since the order tensor (2.1) and (2.2) is a symmetric traceless second rank tensor it also couples with the strain rate in the linear regime and in analogy with equations (2.7a-c) we have:

$$\langle \delta S \rangle = \langle \delta Q_{11} \rangle = \chi_1 \gamma \cos 2\theta, \tag{2.8a}$$

$$\langle \delta Q_{22} \rangle = \chi_2 \gamma \cos 2\theta \tag{2.8b}$$

and

$$\langle \delta Q_{33} \rangle = \chi_3 \gamma \cos 2\theta, \tag{2.8c}$$

where $\langle \delta Q_{\alpha\alpha} \rangle = \langle Q_{\alpha\alpha} \rangle - Q_{\alpha\alpha eq}$, where $\{\langle Q_{\alpha\alpha} \rangle; \alpha = 1,2,3\}$ are the ensemble averages of the order tensor elements, hence the angular brackets, and $\{Q_{\alpha\alpha eq}; \alpha = 1,2,3\}$ are the corresponding equilibrium values and $\chi_1$, $\chi_2$ and $\chi_3$ are cross coupling coefficients between the strain rate and the change of the order tensor It is possible to derive Green-Kubo relations for these coefficients [7]. The effect of this cross coupling is maximal in the zero and 90 degree orientations

and minimal in the ±45 degree orientations. In a nematic liquid crystal the effect of this cross coupling is very small since the order parameter is rather large. In an isotropic liquid consisting of linear molecules such as alkane chains this cross coupling gives rise to an order tensor when the system is undergoing shear flow since the velocity field in this case is a sum of a rotational and an elongational velocity field [2, 3]. This ordering causes shear birefringence.

**2c. Equations of motion**

In a general planar elongational flow where the angle between the elongation direction and the *x*-axis is equal to $\varphi$ the velocity gradient becomes $\nabla\mathbf{u} = \gamma(\mathbf{e}'_x\mathbf{e}'_x - \mathbf{e}'_z\mathbf{e}'_z)$, where $\mathbf{e}'_x = \mathbf{e}_x\cos\varphi - \mathbf{e}_z\sin\varphi$ and $\mathbf{e}'_z = \mathbf{e}_x\sin\varphi + \mathbf{e}_y\cos\varphi$ are the elongation and contraction directions, respectively. Inserting this gradient in the SLLOD equations of motion [9-12] gives

$$\dot{\mathbf{r}}_i = \frac{\mathbf{p}_i}{m} + \mathbf{r}_i\cdot\nabla\mathbf{u} = \frac{\mathbf{p}_i}{m} + \gamma\mathbf{r}_i\cdot(\mathbf{e}'_x\mathbf{e}'_x - \mathbf{e}'_z\mathbf{e}'_z) \tag{2.9a}$$

and

$$\dot{\mathbf{p}}_i = \mathbf{F}_i - \mathbf{p}_i\cdot\nabla\mathbf{u} - \boldsymbol{\beta} = \mathbf{F}_i - \gamma\mathbf{p}_i\cdot(\mathbf{e}'_x\mathbf{e}'_x - \mathbf{e}'_z\mathbf{e}'_z) - \xi\mathbf{p}_i - \boldsymbol{\beta}, \tag{2.9b}$$

where $\mathbf{r}_i$ and $\mathbf{p}_i$ are the position and peculiar momentum of molecule *i*, $\mathbf{F}_i$ is the force exerted on molecule *i* by the other molecules, *m* is the molecular mass, **u** is the streaming velocity and $\gamma$ is the strain rate. The multiplier **β** is a proportional feedback multiplier added to keep the linear momentum constant since it tends to drift [25]. If the arithmetic were exact, this multiplier would remain exactly zero, however, in practice it remains very small and its influence on the ensemble averages of phase functions and time correlations functions is negligible. The thermostatting multiplier $\xi$ is determined by the requirement that the peculiar kinetic energy should be a constant of motion,

$$\xi = \frac{\sum_{i=1}^{N}\left[\mathbf{F}_i\cdot\mathbf{p}_i - \gamma\mathbf{p}_i\cdot(\mathbf{e}'_x\mathbf{e}'_x - \mathbf{e}'_z\mathbf{e}'_z)\cdot\mathbf{p}_i\right]}{\sum_{i=1}^{N}\mathbf{p}_i^2}. \tag{2.10}$$

When these equations are used in practice special periodic boundary conditions must be used. They are easy to implement in an existing molecular dynamics simulation program but it is somewhat complicated to derive them, so they are explained in the next section.

Since the molecules consist of rigid ellipsoids of revolution it is convenient to employ the Euler equations in angular space,

$$I\dot{\boldsymbol{\omega}}_i = \boldsymbol{\Gamma}_i, \tag{2.11}$$

where $I$ is the moment of inertia around the axes perpendicular to the axis of revolution, $\boldsymbol{\omega}_i$ is the angular velocity of molecule $i$ and $\boldsymbol{\Gamma}_i$ is the torque exerted on molecule $i$ by the other molecules. The relation between the rate of change of the molecular axis vectors $d\hat{\mathbf{u}}_i / dt$ and the molecular angular velocity is expressed in terms of quaternions [26].

Since many relations of liquid crystals become simpler when they are expressed in a director based coordinate system it is convenient to fix the director in space so that the coordinate system becomes an inertial frame. This can be done by adding two Lagrangian constraint torques to the Euler equations [20],

$$I\dot{\boldsymbol{\omega}}_i = \boldsymbol{\Gamma}_i + \lambda_x \frac{\partial \Omega_x}{\partial \boldsymbol{\omega}_i} + \lambda_y \frac{\partial \Omega_y}{\partial \boldsymbol{\omega}_i}, \tag{2.12}$$

where $\lambda_x$ and $\lambda_y$ are Lagrangian constraint multipliers determined in such a way that the director angular acceleration becomes a constant of motion. If the initial director angular acceleration and velocity are equal to zero the director will remain fixed in space for all subsequent times.

When the viscosities are evaluated, various element of the pressure tensor are calculated. In this case, the Irving and Kirkwood expression [27] for the pressure tensor is used,

$$\mathbf{P} = \sum_{i=1}^{N} \frac{\mathbf{p}_i \mathbf{p}_i}{m} - \sum_{i=1}^{N} \sum_{j=i+1}^{N-1} \mathbf{r}_{ij} \mathbf{F}_{ij}, \tag{2.13}$$

where $\mathbf{r}_{ij} = \mathbf{r}_j - \mathbf{r}_i$ is the distance vector between molecule $i$ and molecule $j$ and $\mathbf{F}_{ij}$ is the force exerted on molecule $i$ by molecule $j$ and $N$ is the number of molecules.

**2.d Periodic boundary conditions for elongational flow**

The most immediate way to handle the periodic boundary conditions for SLLOD equations (2.9) is to use a periodic lattice of rectangular simulation cells expanding in the $x$-direction and contracting in the $z$-direction, *i.e.* $\varphi = 0$, under constant volume whereby the cells become rectangular parallelepipeds. However, then the simulation must cease when the width in the $z$-direction has diminished to twice the range of the intermolecular interaction potentials, so that there this a time limit of the simulation length for a given system size. This difficulty was circumvented by Daivis and Todd [10, 11] and by Baranyai and Cummings [12], who devised a method for handling the periodic boundary conditions that allows simulations of planar elongational flow of arbitrary length and that is easy to implement. However, the derivation of the method is rather complicated, so only a simplified explanation on the

practical application will be given here, for a detailed derivation the reader is referred to the references [10-13].

The method is based on two observations: Firstly, a theorem of Kraynik and Reinelt [13] according to which there is more than one equivalent representation of a two-dimensional periodic lattice. Consider a periodic lattice of quadratic unit cells, six of which arranged three by two are depicted in fig. 2. Then a parallelogram P where the vectors of the sides are $L_0(2\mathbf{e}_x + \mathbf{e}_z)$ and $L_0(\mathbf{e}_x + \mathbf{e}_z)$, where $L_0$ is the length of the sides of the quadratic unit cells, can be constructed. This parallelogram partially covers the six periodic copies 1 to 6 of the quadratic unit cells. The part of P outside the quadratic unit cell 1 can be divided into three triangles a', b' and c' located in the quadratic unit cells 2, 4 and 5, respectively. These triangles are equivalent to the triangles a, b and c located in unit cell 1. The triangles a, b and c together with the remaining triangle of P in unit cell 1 completely fill this cell without overlapping or leaving any empty space. Thus a periodic lattice of these parallelograms and the periodic lattice of quadratic unit cells are equivalent and there is a 1:1 mapping between them. The initial quadratic unit cell can be transformed to the parallelogram P by the transformation matrix,

$$\mathbf{M} = \begin{pmatrix} 2 & 1 \\ 1 & 1 \end{pmatrix}. \tag{2.14}$$

Note, however, that the parallelogram P is not unique. Any symmetric matrix with integer elements and a determinant equal to unity transforms the quadratic unit cells into parallelograms forming an equivalent periodic lattice.

Secondly, if the elongation and contraction directions are oblique relative to the sides of the quadratic unit cells of the initial lattice, this lattice will be transformed to a lattice of parallelograms. Then, if the eigenvectors of the matrix $\mathbf{M}$ are chosen as the elongation and contraction directions, $\mathbf{e}'_x$ and $\mathbf{e}'_z$, it can be shown that the initial quadratic lattice eventually will become an equivalent lattice of the parallelograms that can be remapped onto the original lattice. It can be shown that this occurs when the elongation and contraction are equal to the largest and smallest eigenvalues, respectively, of $\mathbf{M}$. Since the elongation is equal to $\exp(\gamma t)$ there is a point in time $t_r$ such that

$$t_r = \frac{1}{\gamma} \ln \lambda, \tag{2.15}$$

where $\lambda = (3 + 5^{1/2})/2$ is the largest eigenvalue of $\mathbf{M}$.

More specifically, at time zero the sides of the initial quadratic unit cells are given by

$$\mathbf{L}_1 = L_0(\cos\varphi \mathbf{e}'_x + \sin\varphi \mathbf{e}'_z) = L_0 \mathbf{e}_x \tag{2.16a}$$

and

$$\mathbf{L}_3 = L_0(-\sin\varphi\mathbf{e}'_x + \cos\varphi\mathbf{e}'_z) = L_0\mathbf{e}_z\,, \tag{2.16b}$$

where $\mathbf{L}_1$ and $\mathbf{L}_3$ denote the sides of the unit cell initially parallel to the *x*- and *z*-directions, respectively and $\cos\varphi = 10^{-1/2}(5+5^{1/2})^{1/2}$ or $\varphi \approx 31.7^{\circ}$.

After a time *t* the system has been elongated by a factor $\exp(\gamma t)$ in the $\mathbf{e}'_x$-direction and contracted by a factor of $\exp(-\gamma t)$ in the $\mathbf{e}'_z$-direction, so that the sides of the unit cells become

$$\mathbf{L}_1(t) = L_0[\cos\varphi\mathbf{e}'_x\exp(\gamma t) + \sin\varphi\mathbf{e}'_z\exp(-\gamma t)] \tag{2.17a}$$

and

$$\mathbf{L}_3(t) = L_0[-\sin\varphi\mathbf{e}'_x\exp(\gamma t) + \cos\varphi\mathbf{e}'_z\exp(-\gamma t)]\,. \tag{2.17b}$$

This means that the unit cells have become parallelograms where the angle $\alpha(t)$ between the *x*-axis and $\mathbf{L}_1(t)$ is given by $\tan\alpha(t) = L_{1z}(t)/L_{1x}(t)$ and it is smaller than $\varphi$. At time $t_r$ the initially quadratic unit cell has been transformed to a parallelogram with the sides

$$\mathbf{L}_1(t_r) = L_0(2\mathbf{e}_x + \mathbf{e}_z) \tag{2.18a}$$

and

$$\mathbf{L}_3(t_r) = L_0(\mathbf{e}_x + \mathbf{e}_z)\,. \tag{2.18b}$$

This is the parallelogram P in fig. 2 and the system can be remapped onto the original cell and the simulation can continue.

It is rather difficult to calculate the distances between the interacting molecules located in different periodic copies in a system composed of parallelograms with bases relative to the *x*-axis. Therefore the system is rotated by an angle $-\alpha(t)$ around the *y*-axis so that the bases of the parallelograms become parallel to *x*-axis and an ordinary monoclinic lattice is obtained where the distances between the interacting pairs can be evaluated without complications. Then the system is rotated back by the angle $\alpha(t)$ to compute the forces and torques and to update the positions and velocities.

## 3. MODEL SYSTEM AND TECHNICAL DETAILS

In order to test the above expressions for the various viscosity coefficients and to determine the preferred director orientation, we have simulated a system composed of molecules interacting via a purely repulsive version of the commonly used Gay-Berne potential [18-20]:

$$U(\mathbf{r}_{12},\hat{\mathbf{u}}_1,\hat{\mathbf{u}}_2)=4\varepsilon(\hat{\mathbf{r}}_{12},\hat{\mathbf{u}}_1,\hat{\mathbf{u}}_2)\left(\frac{\sigma_0}{r_{12}-\sigma(\hat{\mathbf{r}}_{12},\hat{\mathbf{u}}_1,\hat{\mathbf{u}}_2)+\sigma_0}\right)^{18}, \tag{3.1}$$

where $\mathbf{r}_{12}=\mathbf{r}_2-\mathbf{r}_1$ is the distance vector from the centre of mass of molecule 1 to the centre of mass of molecule 2, $\hat{\mathbf{r}}_{12}$ is the unit vector in the direction of $\mathbf{r}_{12}$ and $r_{12}$ is the length of $\mathbf{r}_{12}$. The parameter $\sigma_0$ is the length of the axis perpendicular to the axis revolution, *i.e.* the minor axis of a prolate ellipsoid of revolution. The strength and range parameters are given by

$$\varepsilon(\hat{\mathbf{r}}_{12},\hat{\mathbf{u}}_1,\hat{\mathbf{u}}_2)=\varepsilon_0\left[1-\chi^2(\hat{\mathbf{u}}_1\cdot\hat{\mathbf{u}}_2)^2\right]^{-1/2}\left\{1-\frac{\chi'}{2}\left[\frac{(\hat{\mathbf{r}}_{12}\cdot\hat{\mathbf{u}}_1+\hat{\mathbf{r}}_{12}\cdot\hat{\mathbf{u}}_2)^2}{1+\chi'\hat{\mathbf{u}}_1\cdot\hat{\mathbf{u}}_2}+\frac{(\hat{\mathbf{r}}_{12}\cdot\hat{\mathbf{u}}_1-\hat{\mathbf{r}}_{12}\cdot\hat{\mathbf{u}}_2)^2}{1-\chi'\hat{\mathbf{u}}_1\cdot\hat{\mathbf{u}}_2}\right]\right\}^2 \tag{3.2a}$$

and

$$\sigma(\hat{\mathbf{r}}_{12},\hat{\mathbf{u}}_1,\hat{\mathbf{u}}_2)=\sigma_0\left\{1-\frac{\chi}{2}\left[\frac{(\hat{\mathbf{r}}_{12}\cdot\hat{\mathbf{u}}_1+\hat{\mathbf{r}}_{12}\cdot\hat{\mathbf{u}}_2)^2}{1+\chi\hat{\mathbf{u}}_1\cdot\hat{\mathbf{u}}_2}+\frac{(\hat{\mathbf{r}}_{12}\cdot\hat{\mathbf{u}}_1-\hat{\mathbf{r}}_{12}\cdot\hat{\mathbf{u}}_2)^2}{1-\chi\hat{\mathbf{u}}_1\cdot\hat{\mathbf{u}}_2}\right]\right\}^{-1/2}, \tag{3.2b}$$

where the parameter $\chi$ is equal to $(\kappa^2-1)/(\kappa^2+1)$, where $\kappa$ is the ratio between the axis of revolution and the axis perpendicular to the axis revolution, $\chi'$ is equal to, $(\kappa'^{1/2}-1)/(\kappa'^{1/2}+1)$ where $\kappa'$ is the ratio of the potential energy minima of the side by side and end to end configurations, and $\varepsilon_0$ denotes the depth of the potential minimum in the cross configuration, where $\hat{\mathbf{r}}_{12}$, $\hat{\mathbf{u}}_1$ and $\hat{\mathbf{u}}_2$ are mutually perpendicular. The parameters $\kappa$ and $\kappa'$ have been given the values 3.0 and 5.0, respectively. Note that the potential is purely repulsive, so there are no potential minima but the value of $\kappa'$ that has been optimised for the attractive Gay-Berne potential has been retained.

The reason why this purely repulsive potential has been chosen is that there are accurate simulation data on the viscosity of a nematic liquid crystal available based on this potential [8]. This is very useful for a comparison with the results obtained in the present work in order to confirm that the algorithm and the computer program are correct. Another advantage is that this potential is very short-ranged, so that it is possible to obtain accurate estimates of the pressure without any corrections for long-ranged interactions. This is important since the viscosity is obtained from the ensemble averages of the pressure tensor components.

The numerical results in the present work are expressed in length, energy, mass and time units of $\sigma_0$, $\varepsilon_0$, $m$, the molecular mass, and $\tau=\sigma_0(m/\varepsilon_0)^{1/2}$. Thus the units of the pressure, temperature, density, strain rate and torque density become $\varepsilon_0/\sigma_0^3$, $\varepsilon_0/k_B$, $\sigma_0^{-3}$, $\tau^{-1}$

and $\varepsilon_0 / \sigma_0^3$. The moments of inertia around the axes perpendicular to the axis of revolution were given the value $m\sigma_0^2$. The system consisted of 12000 molecules. The equations of motion were integrated by a fourth order Gear predictor–corrector method with a time step of $0.001 \times \tau \ln(3+5^{1/2})/2 \approx 0.0009624\tau$. Then, according to equation (2.15), there will be $2 \times 10^5$, $4 \times 10^5$ and $8 \times 10^5$ timesteps between the remapping of the unit cells when strain rates of $0.005\,\tau^{-1}$, $0.0025\,\tau^{-1}$ and $0.00125\,\tau^{-1}$ are applied. The cutoff radius beyond which the forces and the torques were set equal to zero was $4.5\sigma_0$. The side of the initial cubic unit cell was equal to 47 $\sigma_0$ which equal to about 15 molecular lengths. In the most elongated state the length of the system is equal to 100 $\sigma_0$ and the width is equal to $20\sigma_0$. Thus the smallest dimension of the system is still equal to more than six molecular lengths. The expressions for the forces and the torques that are very complicated are given in ref. [28]. In order to decrease the work needed to create the neighbour list, a cell code was used. The system that we simulate is rather large, so the computational work needed to integrate the equations of motion is too great for an ordinary work station. Therefore we used a replicated data code that we ran on a parallel processor.

## 4. CALCULATIONS, RESULTS AND DISCUSSION

Among other things there are four problems that can be studied by simulating elongational flow of liquid crystal model systems: Firstly, it is possible to determine how the liquid crystal orients relative to the elongation and contraction directions, secondly, it is possible to evaluate the shear viscosities, thirdly the influence of the strain rate on the order parameter can be analysed and finally it is possible to study the irreversible entropy production as a function of the director alignment.

Beginning with the first mentioned problem, it can be noted that, when no external torques act on the liquid crystal, the antisymmetric pressure tensor is equal to zero. According eq. (2.7e) this is the case for the zero degree and the 90 degree orientations, *i.e.* when the director is parallel to the elongation direction or to the contraction direction. In order to determine which one of these directions that is preferred, an elongational velocity field was applied and the director was left free to assume any orientation. Then the angular distribution of the director was obtained by accumulating a bar chart where the order number of the bar is proportional to the centre of an interval of angles between the director and the elongation direction and the height of the bar is proportional to the number of times the director falls into this

interval. A strain rate $\gamma$ of $0.005\,\tau^{-1}$ was applied and the bar chart was formed during a run length of 100 million timesteps. The director orientation was evaluated every fifth timestep and the widths of the angular intervals were 0.25 degrees. The result is shown in fig. 3, where it can be deduced that there is an approximately Gaussian distribution of the director orientation around the zero degree orientation or the elongation direction. If simulations are started with the director oriented in another direction than the elongational direction it moves to this direction or at least close to this direction.

Another way of determining the preferred director orientation is to use the Lagrangian constraint algorithm (2.12) to fix the director at different angles $\theta'$ relative to the elongation direction $\mathbf{e}'_x$ to evaluate the torques needed to keep the director at these angles. Then, as explained in section 2b and in fig. 1, $\theta'$ is positive for a clockwise rotation of the director around the *y*-axis from $\mathbf{e}'_x$ and a positive torque rotates the director clockwise. The director was fixed at angles between -90 and +90 degrees at intervals of 15 degrees between the director and the elongation direction at strain rates of $0.00125\,\tau^{-1}$, $0.0025\,\tau^{-1}$ and $0.005\,\tau^{-1}$. The results are shown in fig. 4 and table 1, where the *y*-component of the antisymmetric pressure $\langle p^a_y \rangle$ is close to zero in the -90, zero and +90 degree orientations, it is negative between -90 and zero degrees and minimal in the -45 degree orientation. It is positive between zero and 90 degrees and maximal in the +45 degree orientation and it follows the relation (2.7e), *i.e.* it is proportional to $\sin 2\theta'$. Since the antisymmetric pressure is equal to the sum of the external torques acting on the system, in this case the Lagrangian constraint torques, a positive torque is required to keep the director oriented in the positive direction and a negative torque is required to keep it oriented in the negative direction. Since the external torque cancels out the torque exerted by the velocity gradient, this means that this gradient acts in the negative direction when the director is displaced in the positive direction from the zero degree orientation and vice versa. Consequently, the orientation parallel to the elongation direction is stable. On the other hand, when the director assumes a positive orientation angle slightly less than 90 degrees relative to the elongation direction, the external torque is positive so that the torque exerted by the velocity field is negative thus twisting the director back towards the zero degree orientation and when the director assumes an orientation angle slightly greater than -90 degrees the external torque is negative so that the torque exerted by the velocity field is positive thus twisting the director towards the zero degree orientation again. Thus the 90 degree orientation is unstable.

Note also that this orientation phenomenon also occurs in ordinary isotropic liquids consisting of elongated molecules, such as for example unbranched alkanes [2-4, 7, 29], when they are sheared, since the shear field is a sum of an elongational velocity field and rotational velocity field. Then the elongational velocity field stretches out the molecules and orients them in the elongation direction, which in the case of shear flow is oriented at an angle of 45 degrees relative to the stream lines, so that a nonequilibrium liquid crystal arises oriented in the 45 degree orientation. This orientation causes shear birefringence since the refractive index becomes different in different directions.

Turning the attention to the second problem - the evaluation of the various shear viscosities - they can be obtained by calculating the ensemble averages of the pressure tensor elements and inserting them in the phenomenological relation (2.7). This was done by using the constraint algorithm (2.12) to fix the director at constant angles $\theta$ relative to the elongation direction so that the pressure tensor elements could be evaluated in a director based coordinate system as functions of $\theta$. Note that the angle $\theta$ is positive for a clockwise rotation of the elongations direction $\mathbf{e}'_x$ from the director, so that $\theta = -\theta'$, see fig. 1. Strain rates of $0.00125\,\tau^{-1}$, $0.0025\,\tau^{-1}$ and $0.005\,\tau^{-1}$ were applied. In figs. 5 and 6 the diagonal elements $\langle \mathring{p}^{s}_{11}(t) \rangle$ and $\langle \mathring{p}^{s}_{33}(t) \rangle$ are displayed as function of $\theta$ for the two lower strain rates and compared to a curve fit to $\cos 2\theta$. It is found that they conform very well to this function as they should according to equation (2.7). It is interesting to note that $\langle \mathring{p}^{s}_{11}(t) \rangle$ and $\langle \mathring{p}^{s}_{33}(t) \rangle$ are almost equal in magnitude but display opposite sign. Thus $\langle \mathring{p}^{s}_{22}(t) \rangle$ must be very small since the sum of the diagonal elements is equal to zero. This is also been found to be the result - $\langle \mathring{p}^{s}_{22}(t) \rangle$ is barely larger than the error bars. The physical reason why $\langle \mathring{p}^{s}_{11}(t) \rangle$ and $\langle \mathring{p}^{s}_{33}(t) \rangle$ are minimal and maximal, respectively, in the zero degree orientation is that the elongation gives rise to a stress response in the opposite direction, *i.e.* the $-\mathbf{e}'_x$ direction, and the contraction give rise to a positive stress response in the $\mathbf{e}'_z$ -direction. The reverse is true in the 90 degree orientation. Meanwhile, the stress in the *y*-direction is more or less unaffected by the flow, so that $\langle \mathring{p}^{s}_{22}(t) \rangle$ remains close to zero In fig. 4 and fig. 7 the antisymmetric pressure $\langle p^{a}_{2}(t) \rangle$ and the off-diagonal element and $\langle \mathring{p}^{s}_{31}(t) \rangle$ are shown and compared to a curve fit to $\sin 2\theta$ since they should be proportional to this quantity according to equation (2.7). Also here the agreement is very good. This shows that the two lower applied strain rates fall within the linear regime and that the linear phenomenological relations (2.7) between the pressure tensor and

the strain rate are fulfilled. The maxima and minima of $\langle \mathring{p}^{s}_{31}(t)\rangle$ as a function of $\theta$ in the ±45 degree orientations are of the same origin as those of $\langle \mathring{p}^{s}_{11}(t)\rangle$ and $\langle \mathring{p}^{s}_{33}(t)\rangle$, namely the normal stress difference caused by the elongation and compression. This can be realized by noting that a shear stress is equivalent to a normal stress difference if the coordinate system is rotated by 45 degrees.

There are four independent elements of the pressure tensor and four independent viscosity coefficients. They can be found by inserting the various calculated pressure tensor elements in the phenomenological relations (2.7) and solving them for the viscosity coefficients,

$$\left(\eta+\frac{\tilde{\eta}_3}{3}\right)=-\frac{1}{2}\lim_{t\to\infty}\frac{\langle \mathring{p}^{s}_{11}(t)\rangle}{\gamma\cos 2\theta}, \tag{4.1a}$$

$$\left(\tilde{\eta}_1+\tilde{\eta}_3\right)/3=-\frac{1}{2}\lim_{t\to\infty}\frac{\langle \mathring{p}^{s}_{22}(t)\rangle}{\gamma\cos 2\theta}, \tag{4.1b}$$

$$\left(\eta+\frac{\tilde{\eta}_1}{3}+\frac{2\tilde{\eta}_3}{3}\right)=\frac{1}{2}\lim_{t\to\infty}\frac{\langle \mathring{p}^{s}_{33}(t)\rangle}{\gamma\cos 2\theta}, \tag{4.1c}$$

$$\left(\eta+\frac{\tilde{\eta}_1}{6}\right)=\frac{1}{2}\lim_{t\to\infty}\frac{\langle \mathring{p}^{s}_{31}(t)\rangle}{\gamma\sin 2\theta} \tag{4.1d}$$

and

$$\tilde{\gamma}_2=-2\lim_{t\to\infty}\frac{\langle p^{a}_{2}(t)\rangle}{\gamma\sin 2\theta}. \tag{4.1e}$$

In principle it is possible obtain estimates of all the shear viscosities by fixing the director at one arbitrary angle except 0, ±45 and ±90 degrees (because either the diagonal or the off-diagonal pressure tensor elements are zero at these angles) and calculating the ensemble averages of the pressure tensor elements. However, if maximal signal-to-noise ratios are to be obtained the diagonal elements should be evaluated at the 0, or ±90 degree orientations where they display maximal absolute magnitudes and the off diagonal elements should be evaluated at the ±45 degree orientations.

However, before the estimates of the viscosities are presented the influence of the strain rate on the order parameter should be discussed. According to equation (2.8a) the change of the order parameter induced by the strain rate is given by $\langle \delta S\rangle = \chi_1\gamma\cos 2\theta$. Thus the order parameter should vary slightly with the orientation angle and the effects should be maximal in the zero and 90 degree orientations and there should be no effect in the 45 degree orientation. By inspecting the order parameter as a function of the orientation angle at the lowest strain rate of $0.00125\,\tau^{-1}$, see table 2a, we find that this parameter is more or less equal

to the equilibrium value of 0.7513 ± 0.0005 in the 45 degree orientation and that it has increased by about 1 percent in the zero degree orientation and decreased by the same amount in the 90 degree orientation. Thus we can conclude that the order parameter at least approximately follows equation (2.8a) and the value of $\chi_1$ is equal to about $7 \pm 1\,\tau$. When the strain rate is doubled to $0.0025\,\tau^{-1}$ the order parameter in the 45 degree orientation is more or less unchanged, in the 0 degree orientation it has increased by 2 percent but in the 90 degree orientation it has decreased by 5 percent, see table 2b. Thus we have the linear behaviour between 0 and 45 degrees but in the angular interval between 45 and 90 degrees nonlinear effects have become important and the absolute value of $\langle \delta S \rangle$ is larger than the predicted by equation (2.8a). Finally when the strain rate is doubled once again to $0.005\,\tau^{-1}$ the order parameter in the 45 degree orientation is still more or less unchanged, in the 0 degree orientation it has increased by 3 percent, so there is still an approximately linear behaviour between 0 and 45 degrees but if the orientation angle is greater than 60 degrees the order parameter decreases to zero and the liquid crystalline order breaks down. Note also that the fact that the order parameter in the 45 degree orientation is more or less equal to the equilibrium value even at the highest strain rate indicates that the influence of the boundary conditions on this parameter is negligible.

These effects on the order parameter should be kept in mind when the values of the combinations of viscosity coefficients on the right hand side of equation (4.1) given in table 2 are examined. Nevertheless, the effects are very small for orientation angles of 45 degrees or less at the two higher strain rates and for any angle at the lowest strain rate, so these results can still be regarded as very accurate and they agree within the error bars with the results obtained with this potential for a system consisting of 256 particles using the ordinary SLLOD equations for shear flow and the Lagrangian constraint algorithm (2.12) to fix the director [8]. However, the relative errors are smaller in the present work since the system is about 50 times larger. For the sake of completeness the values of each one of the shear viscosities $\eta, \tilde{\eta}_1$ and $\tilde{\eta}_3$ and the cross coupling coefficient $\tilde{\gamma}_2$ are given in table 3.

It can be concluded that simulation of elongational flow together with appropriate boundary conditions and the Lagrangian constraint algorithm (2.12) is a powerful and accurate method to obtain shear viscosities of nematic liquid crystals.

Knowing the values of the shear viscosities makes it possible to study the irreversible entropy production as a function of the alignment angle. In the case of elongational flow the

only thermodynamic force is the strain rate and the conjugate thermodynamic flux is the symmetric traceless pressure so that the irreversible entropy production (2.4) simplifies to:

$$\sigma = -\frac{1}{T}\left\langle \overset{\circ}{\mathbf{P}}^{s} \right\rangle : (\overset{\circ}{\nabla}\mathbf{u})^{s} = -\frac{1}{T}\left[\left(\langle \mathring{p}_{11}^{s}\rangle - \langle \mathring{p}_{33}^{s}\rangle\right)\cos 2\theta - 2\langle \mathring{p}_{31}^{s}\rangle \sin 2\theta\right]\gamma$$

$$= \frac{1}{T}\left(4\eta + \frac{2\tilde{\eta}_1}{3} + 2\tilde{\eta}_3 \cos^2 2\theta\right)\gamma^2 . \qquad (4.2)$$

This expression is minimal in the zero and ±90 degree orientations and maximal at the ±45 degree orientations when $\tilde{\eta}_3$ is negative and vice versa when this coefficient is positive. In the present case $\tilde{\eta}_3$ was found to be negative, see table 3a-b. This means that the entropy production is minimal at the zero degree and 90 degree orientations, where the former is the preferred stable orientation. Thus the director assumes the orientation that minimises the entropy production. It could seem counterintuitive that there are equally deep minima both at the zero degree orientation and the 90 degree orientation. However, in the zero degree orientation where the director is parallel to the elongation direction, the molecules also are oriented in this direction to a large extent when the order parameter is high. This means that they can pass each other very easily since they are streamlined in this direction. This lowers the overall friction in the system and decreases the entropy production. In the 90 degree orientation a large portion of the molecules are more or less parallel to the contraction direction, so that the friction of the flow in this direction is decreased thus decreasing the overall friction. On the other hand, in the 45 degree orientation the molecules are to a large extent oriented in this direction relative the steam lines both in the elongation and contraction directions. This means that side-to-side collisions become more frequent, so that the friction and thereby the entropy productions increases.

Since the irreversible entropy production must be positive according to the second law of thermodynamics, it follows that the three shear viscosities must satisfy the following inequality for the preferred alignment angle $\theta_0$,

$$4\eta + \frac{2\tilde{\eta}_1}{3} + 2\tilde{\eta}_3 \cos^2 2\theta_0 > 0 . \qquad (4.3)$$

Finally, it is interesting to note that nematic liquid crystals also in other cases tend to assume the orientation relative to an external dissipative field such as a velocity gradient or a temperature gradient where the irreversible entropy production is minimal. This has been noted both in simulations [8, 30] and experimentally [31] for nematic liquid crystals undergoing shear flow, where the director approximately assumes an angle relative to the stream lines that

minimises the irreversible entropy production. When a nematic phase of a model system consisting of elongated molecules is subjected to a temperature gradient the director orients perpendicularly to this gradient [32] whereby the heat flow and thus the entropy production is minimised since the perpendicular component of the heat conductivity is smaller than the parallel component of this conductivity. The reverse has been found for liquid crystals consisting of discotic molecules.

## 5. CONCLUSION

A nematic phase of a liquid crystal model system based on a purely repulsive version of the Gay-Berne potential undergoing planar elongational flow has been investigated by molecular dynamics simulation in order to determine the preferred alignment angle and the shear viscosities by substituting the elongational velocity field into the SLLOD equations of motion. Then a particular problem that must be handled correctly is the periodic boundary conditions. The simplest way of doing this for elongational flow is to use a lattice of rectangular unit cells expanding in one direction and contracting in the perpendicular direction. However, then the simulation must cease when the system has contracted to a dimension equal to twice the range of the intermolecular interaction potential. Therefore, a more advanced method developed by Daivis and Todd and by Baranyai and Cummings based on the Kraynik-Reinelt boundary conditions [10-13] was used where the elongation and contraction directions are oblique relative to the sides of the initial quadratic simulation cell. This causes an initial quadratic periodic lattice to be transformed to a lattice of parallelograms. For certain angles between the elongation and contraction directions and the sides of the initial quadratic simulation cell the parallelograms will after a certain time form a periodic lattice that is equivalent to the initial periodic quadratic lattice and then parallelograms can be remapped onto the initial quadrates so that the simulation can continue indefinitely.

The preferred orientation of the director relative to the elongation direction was determined by leaving the director free to assume any direction. This led to that an approximately Gaussian angular distribution of the director around the elongation direction was obtained. In order to crosscheck this result a Lagrangian constraint algorithm was applied to fix the director at angular intervals of 15° between -90° and +90° relative to the elongation direction and the angular dependence of the antisymmetric pressure tensor was evaluated. This quantity is equal to the sum of the external torques exerted on the system, in this case the Lagrangian constraint torques, and they are equal in magnitude but opposite in sign compared to the torque exerted by the strain rate. It was found that the antisymmetric pressure obeys the linear

phenomenological relation (2.7) according to which the torque is zero in the parallel and perpendicular orientations relative to the elongation direction. However, if the director deviates from the elongation direction, the strain rate exerts a torque twisting it back to this orientation but if it deviates from the contraction direction, the torque exerted by the strain rate twists the director away from this direction back to the parallel orientation. Thus the parallel orientation is stable and the perpendicular orientation is unstable.

Then the shear viscosities were evaluated by calculating the various elements of the pressure tensor and comparing them with the linear phenomenological relations between the pressure and the strain rate for three different strain rates in the linear regime. According to these relations the diagonal pressure tensor elements are proportional to $\cos 2\theta$ where $\theta$ is the angle between the director and the elongation direction and the off-diagonal element and the antisymmetric pressure are proportional to $\sin 2\theta$ and this was found to be the case within relative errors of a few percent. The estimated values of the shear viscosities agreed very well with estimates from conventional shear flow simulations and from Green-Kubo relations. Thus simulation of elongational flow is a powerful and accurate method to obtain shear viscosities of nematic liquid crystals.

Since the order tensor and the strain rate both are symmetric traceless second rank tensors, there is a linear cross coupling between them. By symmetry the relation between the change of the order tensor and the strain rate is proportional to $\cos 2\theta$ in the linear regime, so that the change of the order tensor and thereby the order parameter should be maximal in the zero degree and 90 degree orientations and there should be no effect in the 45 degree orientation. This linear behaviour is observed over the whole angular interval at a strain rate of $0.00125\ \tau^{-1}$. At the two higher strain rates of $0.0025\,\tau^{-1}$ and $0.005\,\tau^{-1}$ the linear behaviour is found between zero and 45 degrees, whereas the order parameter decreases more than predicted by the linear relation for orientation angles greater than 45 degrees, and when the largest strain rate is applied the liquid crystalline order breaks down if the orientation angle is greater than 60 degrees. However, at the lowest strain rate and for orientation angles of 45 degrees or less at the higher strain rates the order parameter changes by at most 2 percent or less so the influence on the estimates of the shear viscosities is very low. Note that this cross coupling gives rise to shear induced alignment and shear birefringence in isotropic liquids under shear since the shear field is the sum of rotational and an elongational velocity field, where the latter field stretches out and orients the molecules.

Finally, the irreversible entropy production was analysed. In the linear regime it is proportional to the sum of a constant and $\tilde{\eta}_3 \cos^2 2\theta$, so that it is maximal or minimal in the zero, ±45 and ±90 degree orientations depending on the sign of the shear viscosity $\tilde{\eta}_3$. In the present case this viscosity was found to be negative, so the entropy production is minimal in the zero degree orientations or in elongational direction and in the 90 degree or contraction direction. However, only the former direction is stable, so this means that the director assumes the orientation that minimises the entropy production. This is an additional example of a nematic liquid crystal orienting in such a way that the irreversible entropy production is minimised. This has also been found in simulations of nematic liquid crystal model systems subject to a temperature gradient where the director orients in such a way that the heat flow is minimised. In shear flow simulations it does not follow directly from the linear phenomenological relations that an orientation minimising the irreversible entropy production is assumed. However, both in simulations and in experimental measurements it has been found that such an angle is approximately assumed.

## Acknowledgement

We gratefully acknowledge financial support from the Knut and Alice Wallenberg Foundation (Project number KAW 2012.0078) and Vetenskapsrådet (Swedish Research Council) (Project number 2013-5171). The simulations were performed using resources provided by the Swedish National Infrastructure for Computing (SNIC) at PDC, HPC2N and NSC.). Finally, we thank professor Peter Daivis for useful advice on the implementation of the Kraynik-Reinelt boundary conditions.

## REFERENCES


1. A. W. Lees and S. F. Edwards, J. Phys., 1972, C 5, 1921.
2. R. Edberg, D. J. Evans and G. P. Morriss, J. Chem. Phys., 1987, **86**, 4555.
3. G. P. Morriss, P. J. Daivis and D. J. Evans, J. Chem. Phys., 1991, **94**, 7420.
4. S. Sarman, P. J. Daivis and D. J. Evans, Phys. Rev. E, 1993, **47**, 1784.
5. D. Baalss and S. Hess, Phys. Rev. Lett., 1986**, 57**, 86.
6. D. Baalss and S. Hess, *Z.* Naturforsch. A: Phys. Sci., 1988, **43**, 662.
7. S. Sarman and D. J. Evans, J. Chem. Phys., 1993, **99**, 9021.
8. S. Sarman, J. Chem. Phys., 1995, **103**, 10378.
9. D. J. Evans and G. P. Morriss, Statistical Mechanics of Nonequilibrium Liquids, Academic Press, London, 1990.
10. B. D. Todd and P. J. Daivis, Phys. Rev. Lett., 1998, **81**, 1118.
11. B. D. Todd and P. J. Daivis, Molecular Simulation, 2007, **33**, 189.
12. A. Baranyai and P. T. Cummings, J. Chem. Phys., 1995, **103**, 10217.
13. A. M. Kraynik and D. A. Reinelt, Int. J. Multiphase Flow, 1992, **18**, 1045.
14. M.L. Matin, P.J. Daivis and B.D. Todd, J. Chem. Phys., 2000**, 113**, 9122.
15. M.L. Matin, P.J. Daivis and B.D. Todd, Computer Physics Communications, 2003, **151**, 35
16. P.J. Daivis, M.L. Matin and B.D. Todd, J. Non-Newtonian Fluid Mech., 2003, **111**, 1
17. P.J. Daivis, M.L. Matin and B.D. Todd, J. Non-Newtonian Fluid Mech., 2007, **147**, 35
18. J. G. Gay and B. J. Berne, J. Chem. Phys., 1981**, 74**, 3316.
19. M. A. Bates and G. R. Luckhurst, J. Chem. Phys., 1996, **104**, 6696.
20. S. Sarman, J. Chem. Phys., 1994, **101**, 480.
21. S. Chandrasekhar, Liquid Crystals, Cambridge University Press, Cambridge, 1992.
22. P. G. DeGennes and J. Prost, The Physics of Liquid Crystals, Clarendon Press, Oxford, 1992
23. Hess, J. Non-Equilib. Thermodyn., 1986, **11**, 175.
24. S. R. de Groot and P. Mazur, Nonequilibrium Thermodynamics, Dover, New York, 1984
25. B. D. Todd and P. J. Daivis, J. Chem. Phys., 2000, **112**, 40.
26. D. J. Evans, Mol. Phys., 1977, **34**, 317.
27. H. Irving and J. G. Kirkwood, J. Chem. Phys., 1950, **18**, 817.
28. S. Sarman and D. J. Evans, J. Chem. Phys., 1993, **99**, 620.

29. J. C. Maxwell, Proc. R. Soc. London, Ser. A, 1873, **22**, 151.
30. S. Sarman, J. Chem. Phys., 1995, **103**, 393.
31. J. Jadzyn and G. Czechowski, J. Phys.: Condens. Matter, 2001, **13**, L261.
32. S. Sarman and A. Laaksonen, Phys. Chem. Chem. Phys., 2014, **16**, 14741.

**FIGURE CAPTIONS**

Fig. 1

The three different coordinate systems: (*i*) the system with the basis vectors $(\mathbf{e}_x, \mathbf{e}_y, \mathbf{e}_z)$ used in the actual calculations and where the omitted *y*-axis is perpendicular to the image plane and points away from the observer, (*ii*) a system obtained by rotation around the *y*-axis with the basis vectors $(\mathbf{e}'_x, \mathbf{e}'_y\, \mathbf{e}'_z)$ where $\mathbf{e}'_x$ is parallel to the elongation direction, $\mathbf{e}'_y = \mathbf{e}_y$ is parallel to the *y*-axis and the contraction direction is parallel to $\mathbf{e}'_z$, and (*iii*) a director based coordinate system with the basis vectors $(\mathbf{e}_1, \mathbf{e}_2\, \mathbf{e}_3)$ obtained by rotation around the *y*-axis where $\mathbf{e}_1$ is parallel to the director $\mathbf{n}$, $\mathbf{e}_2 = \mathbf{e}'_y = \mathbf{e}_y$ is parallel to the *y*-axis, and $\mathbf{e}_3 = \mathbf{n} \times \mathbf{e}_2$. The angle between $\mathbf{e}'_x$ and $\mathbf{e}_x$ is denoted by $\varphi$ and it is positive for a rotation clockwise around the *y*-axis from $\mathbf{e}_x$ to $\mathbf{e}'_x$ so it is negative in the figure. The angle between $\mathbf{n}$ and $\mathbf{e}'_x$ is denoted by $\theta'$ and it is positive for a rotation clockwise of $\mathbf{n}$ from $\mathbf{e}'_x$ around the *y*-axis, so it is also negative in the figure. Finally, the angle between the elongation direction $\mathbf{e}'_x$ and the $\mathbf{e}_1$ in the director based coordinate system is denoted by $\theta$ and it is positive when $\mathbf{e}'_x$ is rotated clockwise from $\mathbf{e}_1$, so it is positive in the figure and $\theta' = -\theta$.

Fig. 2

The parallelogram (dashed lines) partially covers the squares (1-6). The triangles a', b' and c' in the parallelogram are periodic copies of the triangles a, b and c in square 1.

Fig. 3

The angular distribution of the director as a function of the angle $\theta'$ between the director and the elongation direction at a strain rate of $0.005\,\tau^{-1}$. The error bars are of the size of the symbols.

Fig. 4

The antisymmetric pressure tensor $\langle p_y^a \rangle$ in the coordinate system with the basis vectors $(\mathbf{e}'_x, \mathbf{e}'_y\, \mathbf{e}'_z)$, where $\mathbf{e}'_x$ is parallel to the elongation direction, as a function of the angle between the director and the elongation direction $\theta'$. Note that this angle is positive when the director is rotated clockwise from the elongation direction and that a positive torque rotates

the director in this direction. The strain rates are $0.0025\,\tau^{-1}$ (squares) and $0.00125\,\tau^{-1}$ (diamonds) and the error bars are of the size of the symbols. The dashed lines are curve fits to $\sin 2\theta'$.

Fig. 5

The pressure tensor component $\langle \overset{\circ}{p}{}^{s}_{11} \rangle$ in a director based coordinate system as a function of the angle $\theta$ between the elongation direction and the director. Note that this angle is equal to $-\theta'$. The strain rates are $0.0025\,\tau^{-1}$ (squares) and $0.00125\,\tau^{-1}$ (diamonds) and the error bars are of the size of the symbols. The dashed lines are curve fits to $\cos 2\theta$.

Fig. 6

As in fig. 5 but the pressure tensor component is $\langle \overset{\circ}{p}{}^{s}_{33} \rangle$.

Fig. 7

As in fig. 5 but the pressure tensor component is $\langle \overset{\circ}{p}{}^{s}_{31} \rangle$ and the dashed lines are curve fits to $\sin 2\theta$.

Fig. 8

The irreversible entropy production divided by the square of the strain rate, $\sigma / \gamma^2$ (diamonds) as a function of the director alignment angle $\theta$ at a strain rate of $0.00125\,\tau^{-1}$. The dashed line is a curve fit to $\cos^2 2\theta$.

**Table captions**

Table 1a

The viscosity combinations obtained by dividing the diagonal elements of the pressure tensor by the factor $2\gamma\cos 2\theta$, *i. e.* $\eta+\tilde{\eta}_3/3=-\langle \overset{\circ}{p}{}^s_{11}\rangle/2\gamma\cos 2\theta$, $(\tilde{\eta}_1+\tilde{\eta}_3)/3=-\langle \overset{\circ}{p}{}^s_{22}\rangle/2\gamma\cos 2\theta$ and $\eta+\tilde{\eta}_1/3+2\tilde{\eta}_3/3=\langle \overset{\circ}{p}{}^s_{33}\rangle/2\gamma\cos 2\theta$, see equation (4.1), evaluated at different angles $\theta$ in a director based coordinate system at a strain rate of $0.00125\,\tau^{-1}$.

Table 1b

As in table 1a but the reduced strain rate is equal to $0.0025\,\tau^{-1}$.

Table 1c

As in table 1a but the reduced strain rate is equal to $0.005\,\tau^{-1}$.

Table 2a

The viscosity combination $\eta+\tilde{\eta}_1/6=\langle \overset{\circ}{p}{}^s_{31}\rangle/2\gamma\sin 2\theta$ and the cross coupling coefficient $\tilde{\gamma}_2=-2\langle p^a_2\rangle/\gamma\sin 2\theta$ and the order parameter $S$ evaluated at different angles $\theta$ in a director based coordinate system at a strain rate of $0.00125\,\tau^{-1}$.

Table 2b

As in table 2a but the strain rate is equal to $0.0025\,\tau^{-1}$.

Table 2c

As in table 2a but the strain rate is equal to $0.005\,\tau^{-1}$.

Table 3a

The shear viscosities $\eta$, $\tilde{\eta}_1$ and $\tilde{\eta}_3$ as functions of $\theta$ in a director based coordinate at a strain rate of $0.00125\,\tau^{-1}$.

Table 3b

As in table 3a but the strain rate is equal to $0.0025\,\tau^{-1}$.

Table 3c

As in table 3a but the strain rate is equal to $0.005\,\tau^{-1}$.

**TABLES**

Table 1a

| $\theta$ | $\eta+\tilde{\eta}_3/3$ | $(\tilde{\eta}_1+\tilde{\eta}_3)/3$ | $\eta+\tilde{\eta}_1/3+2\tilde{\eta}_3/3$ |
|---|---|---|---|
| 0º | 2.74±0.05 | -0.02±0.07 | 2.72±0.08 |
| 15º | 2.72±0.06 | -0.07±0.03 | 2.65±0.05 |
| 30º | 2.70±0.13 | -0.0±0.1 | 2.68±0.06 |
| 60º | 2.82±0.30 | -0.09±0.08 | 2.79±0.09 |
| 75º | 2.92±0.40 | -0.12±0.05 | 2.69±0.04 |
| 90º | 2.79±0.02 | -0.06±0.04 | 2.73±0.02 |

Table 1b

| $\theta$ | $\eta+\tilde{\eta}_3/3$ | $(\tilde{\eta}_1+\tilde{\eta}_3)/3$ | $\eta+\tilde{\eta}_1/3+2\tilde{\eta}_3/3$ |
|---|---|---|---|
| 0º | 2.74±0.05 | -0.02±0.06 | -2.72±0.08 |
| 15º | 2.72±0.04 | -0.05±0.03 | -2.66±0.04 |
| 30º | 2.69±0.05 | -0.04±0.07 | -2.65±0.06 |
| 60º | 2.54±0.04 | -0.11±0.06 | -2.70±0.06 |
| 75º | 2.84±0.03 | -0.08±0.04 | -2.76±0.04 |
| 90º | 2.94±0.03 | 0.00±0.05 | -2.94±0.06 |

Table 1c

| $\theta$ | $\eta+\tilde{\eta}_3/3$ | $(\tilde{\eta}_1+\tilde{\eta}_3)/3$ | $\eta+\tilde{\eta}_1/3+2\tilde{\eta}_3/3$ |
|---|---|---|---|
| 0º | 2.67±0.03 | -0.05±0.03 | 2.62±0.02 |
| 15º | 2.66±0.02 | -0.06±0.03 | 2.61±0.02 |
| 30º | 2.67±0.04 | -0.07±0.02 | 2.61±0.02 |
| 60º | 2.62±0.03 | -0.07±0.03 | 2.55±0.02 |

Table 2a

| $\theta$ | $\eta + \tilde{\eta}_1 / 6$ | $\tilde{\gamma}_2$ | $S$ |
|---|---|---|---|
| 0º | | | 0.7576±0.0004 |
| 15º | 5.2±0.1 | -13.9±0.3 | 0.7565±0.0001 |
| 30º | 5.2±0.1 | -13.8±0.2 | 0.7543±0.0004 |
| 45º | 5.1±0.1 | -13.6±0.3 | 0.749±0.001 |
| 60º | 5.4±0.1 | -14.2±0.1 | 0.744±0.001 |
| 75º | 5.12±0.1 | -13.7±0.2 | 0.739±0.001 |
| 90º | | | 0.740±0.001 |

Table 2b

| $\theta$ | $\eta + \tilde{\eta}_1 / 6$ | $\tilde{\gamma}_2$ | $S$ |
|---|---|---|---|
| 0º | | | 0.7622±0.0003 |
| 15º | 5.19±0.04 | -13.9±0.1 | 0.7625±0.0004 |
| 30º | 5.21±0.05 | -13.9±0.2 | 0.7576±0.0003 |
| 45º | 5.16±0.04 | -13.7±0.1 | 0.7497±0.0003 |
| 60º | 5.27±0.03 | -13.9±0.1 | 0.738±0.0012 |
| 75º | 5.1±0.1 | -13.6±0.1 | 0.719±0.002 |
| 90º | | | 0.709±0.002 |

Table 2c

| $\theta$ | $\eta + \tilde{\eta}_1 / 6$ | $\tilde{\gamma}_2$ | $S$ |
|---|---|---|---|
| 0º | | | 0.7740±0.0002 |
| 15º | 5.2±0.1 | -14.1±0.2 | 0.7714±0.0004 |
| 30º | 5.22±0.02 | -14.00±0.04 | 0.7640±0.0003 |
| 45º | 5.18±0.02 | -13.70±0.03 | 0.7502±0.0003 |
| 60º | 5.14±0.03 | -13.4±0.2 | 0.7203±0.003 |

Table 3a

| | $\eta$ | $\tilde{\eta}_1$ | $\tilde{\eta}_3$ |
|---|---|---|---|
| 15º | 4.41±0.10 | 4.8±0.2 | -5.1±0.2 |
| 30º | 4.38±0.07 | 4.9±0.5 | -5.0±0.2 |
| 60º | 4.47±0.08 | 4.4±0.6 | -4.8±0.3 |
| 75º | 4.44±0.08 | 4.5±0.3 | -4.9±0.2 |

Table 3b

| | $\eta$ | $\tilde{\eta}_1$ | $\tilde{\eta}_3$ |
|---|---|---|---|
| 15º | 4.38±0.08 | 5.0±0.2 | -5.0±0.10 |
| 30º | 4.43±0.07 | 5.0±0.4 | -5.1±0.2 |
| 60º | 4.44±0.07 | 5.0±0.3 | -5.5±0.2 |
| 75º | 4.39±0.05 | 4.2±0.3 | -4.7±0.2 |

Table 3b

| | $\eta$ | $\tilde{\eta}_1$ | $\tilde{\eta}_3$ |
|---|---|---|---|
| 15º | 4.40±0.04 | 5.0±0.1 | -5.2±0.1 |
| 30º | 4.40±0.02 | 5.0±0.1 | -5.2±0.1 |
| 60º | 4.3±0.1 | 4.9±0.2 | -5.1±0.1 |

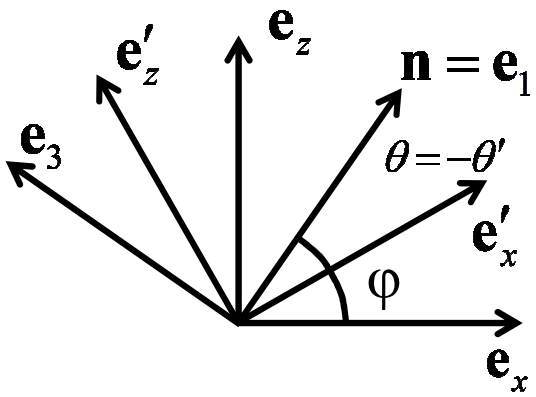


Fig. 1

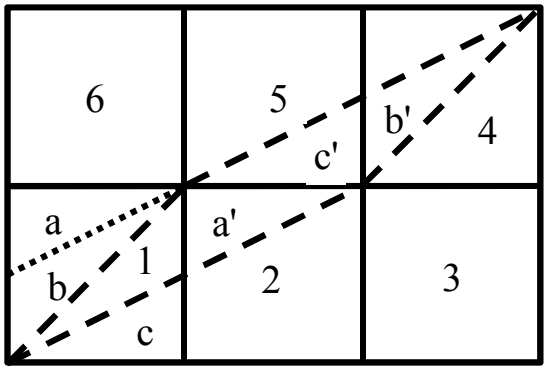


Fig. 2

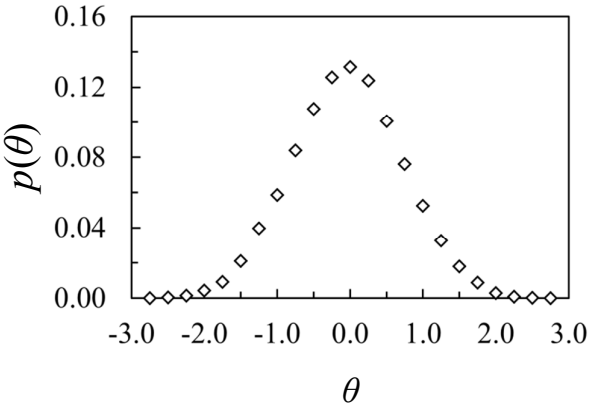


Fig. 3

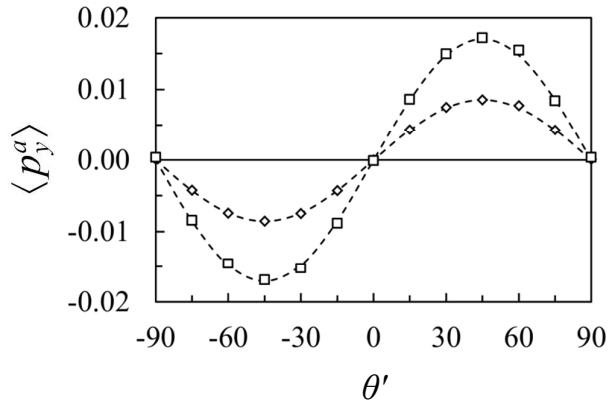


Fig. 4

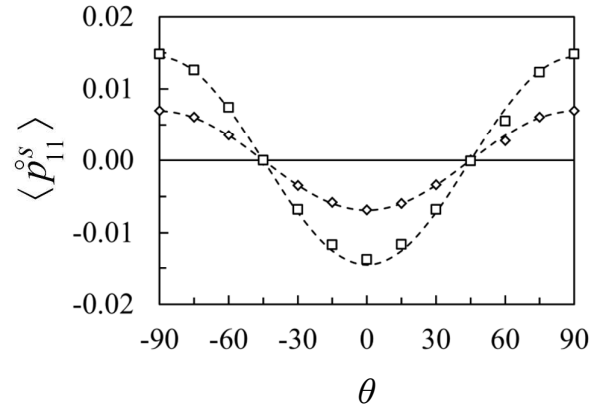


Fig. 5

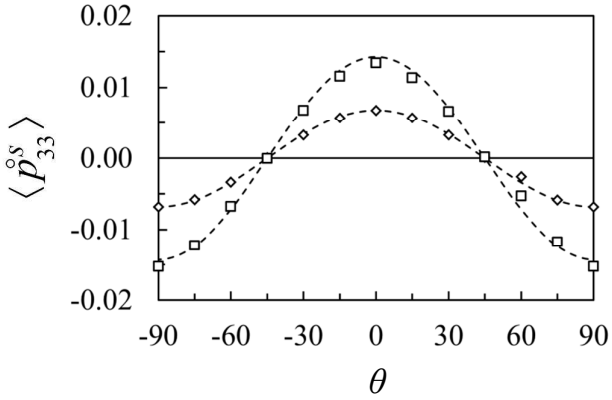


Fig. 6

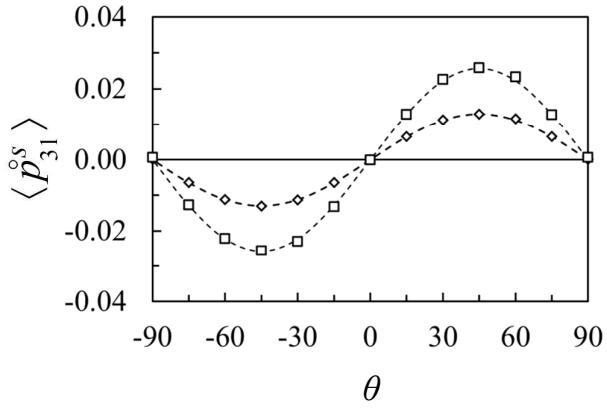


Fig. 7

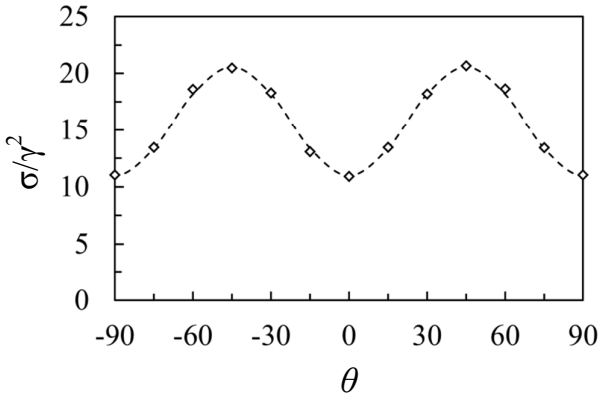


Fig. 8